Nonlinear saturation of collisionless trapped electron mode turbulence: Zonal flows and zonal density[a)]

Jianying Lang,[b)] Scott E. Parker, and Yang Chen
Center for Integrated Plasma Studies, Department of Physics, University of Colorado at Boulder, Boulder, Colorado 80309, USA

(Received 16 November 2007; accepted 22 January 2008; published online 13 March 2008)

Gyrokinetic δf particle simulation is used to investigate the nonlinear saturation mechanisms in collisionless trapped electron mode (CTEM) turbulence. It is found that the importance of zonal flow is parameter-sensitive and is well characterized by the shearing rate formula. The effect of zonal flow is empirically found to be sensitive to temperature ratio, magnetic shear, and electron temperature gradient. For parameters where zonal flow is found to be unimportant, zonal density (purely radial density perturbations) is generated and expected to be the dominant saturation mechanism. A toroidal mode-coupling theory is presented that agrees with simulation in the initial nonlinear saturation phase. The mode-coupling theory predicts the nonlinear generation of the zonal density and the feedback and saturation of the linearly most unstable mode. Inverse energy cascade is also observed in CTEM turbulence simulations and is reported here. © *2008 American Institute of Physics*. [DOI: 10.1063/1.2884036]

I. INTRODUCTION

Collisionless trapped electron modes (CTEM) are expected to be an important contributor to anomalous transport in tokamak plasmas when the density gradient drive is dominant over the ion temperature gradient drive. CTEM turbulence has been investigated extensively in theoretical[1,2] and simulation studies.[3–6] There is also experimental evidence that CTEM plays an important role in both particle and electron thermal diffusivities.[3,7,8] Here, the nonlinear saturation mechanisms are investigated in CTEM turbulence using gyrokinetic particle simulation. In our previous work,[6] the dependence of CTEM driven transport on important local plasma parameters was studied. In this paper, we explore two CTEM saturation mechanisms, namely zonal shear flow suppression and a new zonal density saturation mechanism. We also investigate inverse cascade in CTEM turbulence.

Large-scale gyrokinetic simulation is an important tool for understanding the nonlinear physics. The simulation studies presented here use a flux-tube geometry. The gyrokinetic particle-in-cell δf code used in our work is a flux-tube version of the GEM code,[9,10] which employs field-line-following coordinates (x,y,z) (Ref. 11) and includes gyrokinetic ions and drift-kinetic electrons. The coordinates (x,y,z) are defined from toroidal coordinates (r,θ,ζ) by $x=r-r_0$, $y=(r_0/q_0)(q\theta-\zeta)$, and $z=q_0R_0\theta$, where R_0 is the major radius at the magnetic axis, r_0 is the minor radius at the center of the simulation domain, $q_0=q(r)$ is the safety factor, x is the radial coordinate, y is the coordinate perpendicular to magnetic field $\mathbf{B}$, and z is the coordinate along the field line. Periodic boundary conditions are applied in the x and y directions and the toroidal boundary condition is applied in the z direction.[11] Using a five-dimensional phase space, the dynamics of both trapped and passing electrons and pitch-angle scattering are included. See further details for the code in Ref. 9. GEM is fully electromagnetic, but only electrostatic simulations are reported here.

In this paper, we show that the suppression of turbulent transport by zonal flows for CTEM is not a universal feature, but is important only in certain parameter regimes. We have systematically studied the effect of zonal flows in suppressing CTEM turbulence using six important local plasma parameters: density gradient R/L_n, electron temperature gradient R/L_{Te}, electron to ion temperature ratio T_e/T_i, magnetic shear $\hat{s}$, safety factor q, and inverse aspect ratio r/R. We find that among them the electron temperature gradient, electron to ion temperature ratio, and magnetic shear can affect the suppression of zonal flows. We also find that the effect of zonal flows in regulating the turbulence is consistent with the $E\times B$ shearing rate.[12,13]

Of particular interest is understanding the saturation mechanism when zonal flows are unimportant. In this paper, we show the generation of zonal density as being responsible for nonlinear saturation when zonal flows are unimportant. In fact, CTEM simulations saturate at comparable levels when zonal flows are either kept or removed from the simulations. In order to understand the stabilization from zonal density, we introduce a simple mode-coupling model in which only a single toroidal mode and its complex conjugate are retained. This mode-coupling model predicts the generation of zonal density and the initial nonlinear saturation level with only one toroidal mode and its complex conjugate are retained in the electrostatic potential, which agrees qualitatively with the simulations.

Besides zonal density generation, we also find energy transfer from the linearly unstable mode with shorter wavelengths to the linearly stable modes with longer wavelengths to be important. The correlation between the downward shift in the averaged wave number and the CTEM saturation is

[a)]Paper NI1 3, Bull. Am. Phys. Soc. **52**, 187 (2007).
[b)]Invited speaker.

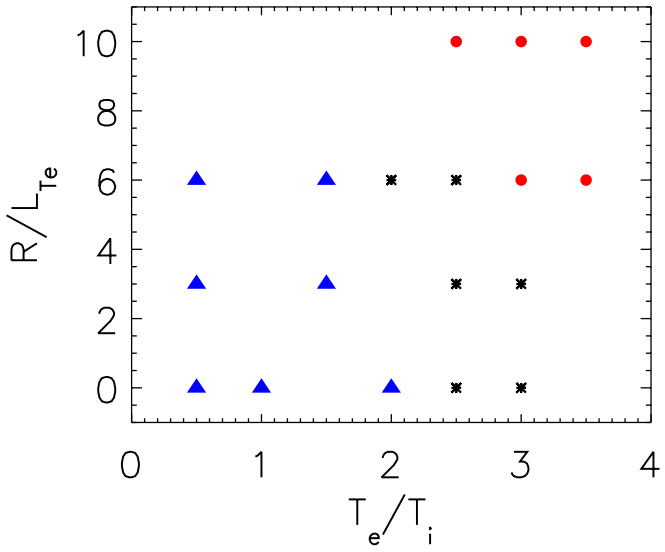

FIG. 1. (Color online) Normalized electron temperature gradient and electron to ion temperature ratio scan for the importance of zonal flows on suppressing the CTEM turbulent transport. Triangles stand for the electron thermal flux increasing more than 2.5 times with zonal flows zeroed out. Asters stand for the electron thermal flux increasing about 2 times with zonal flows zeroed out. Circles stand for the difference caused by zonal flows being less than 30%.

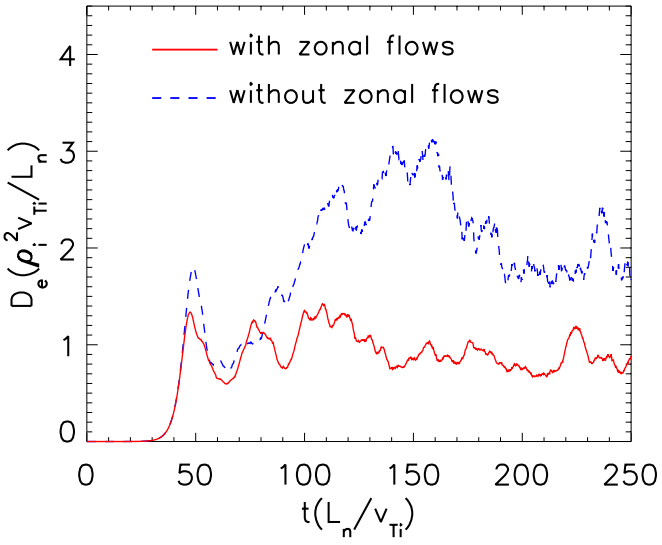

FIG. 2. (Color online) Comparison of the time evolution of particle diffusivities for magnetic shear $\hat{s}=1.2$ (other parameters listed in Sec. II) between with zonal flows (solid line) and without zonal flows (dashed line).

consistent with the numerical observations in ion temperature gradient turbulence (ITG) simulations.[14,15]

This paper is organized as follows. Section II reports the parameter dependence of the suppression effect of zonal flows on the CTEM turbulent transport. In Sec. III, we analyze the generation of zonal density in the presence of a single toroidal mode and the feedback on the primary mode and nonlinear saturation, using a mode-coupling model. In Sec. IV, we compare the mode-coupling theory to nonlinear simulations. In Sec. V, we discuss the inverse energy cascade in CTEM turbulent simulations.

II. IMPORTANCE OF ZONAL FLOW AND ZONAL DENSITY IN CTEM TURBULENCE

Zonal flows are known to be the dominant saturation mechanism for the ITG turbulence.[16–19] For CTEM, the effect of zonal flows is found to be somewhat ambiguous. The work by Dannert *et al.* using the GENE code shows that zonal flows are unimportant for the saturation,[4] whereas nonlinear simulations with the GS2 code reported by Ernst *et al.* show there is a nonlinear upshift in the TEM critical density gradient, caused by zonal flows.[3] Our simulations indicate that the importance of zonal flows for CTEM transport depends on the local plasma parameters. We have carried out many simulations with varying local plasma parameters, comparing a simulation that includes the self-generated zonal flows with a simulation where the zonal flow is zeroed out, and observing the difference in the turbulent transport obtained. We have found the two most important parameters affecting the zonal flow suppression effect: R/L_{Te} and T_e/T_i. A two-dimensional scan is performed for these two parameters. The R/L_{Te} and T_e/T_i are varied from 0 to 10 and from 0.5 to 3.5, respectively. Other parameters are based on a previous CTEM publication[6] with ion temperature gradient $R/L_{Ti}=0$, density gradient $R/L_n=10$, safety factor $q_0=1.4$, magnetic shear $\hat{s}=0.8$, plasma to magnetic pressure $\beta\equiv 2(T_e+T_i)\mu_0 n_0/B_0^2=0.0001$, ion to electron mass ratio $m_p/m_e=1837$, and inverse aspect ratio $r/R=0.16$. The split-weight parameter is $\epsilon_g=0.1$ and the time step $\Omega_i\triangle t=2$, where Ω_i is the ion gyrofrequency. The simulation box size is $l_x=128\rho_i$, $l_y=64\rho_i$. The grid resolution is $\triangle x=\rho_i$, $\triangle y=\rho_i$, and 64 particles per cell per species. Length is measured by the ion gyroradius $\rho_i=\sqrt{T_i/m_i}/\Omega_i$ and time is normalized with L_n/V_{Ti}, where $V_{Ti}=\sqrt{T_i/m_i}$ is the ion thermal velocity.

Figure 1 shows the $2D$ plot of the changes in electron thermal flux with and without zonal flows at various values of R/L_{Te} and T_e/T_i. Different symbols represent the different variation in the CTEM turbulent transport level caused by artificially zeroing out the zonal flows. Triangles indicate the electron thermal flux increases more than 2.5 times without zonal flows. Asters indicate the electron thermal flux increases about 2 times without zonal flows. Circles indicate a difference of less than 30% due to the zonal flows. Figure 1 shows that the shearing suppression due to zonal flows is weaker for cold ions as well as steeper electron temperature gradient. On the other hand, $E\times B$ shearing rate $\omega_{E\times B}$ resulting from the zonal flow[12,13] can be calculated from the simulation. At $T_e/T_i=3$ and $R/L_{Te}=6$, the ratio of $\omega_{E\times B}$ to the linear growth rate γ_L is 0.2 and zeroing out the self-generated zonal flows shows negligible effects on the transport level. At $T_e/T_i=1$ and $R/L_{Te}=0$, $\omega_{E\times B}$ is comparable to the linear growth rate γ_L and there is more than a factor 3 difference in the transport level between with and without zonal flows. Therefore, the results are consistent with the shearing rate criterion.

We note that the variation of magnetic shear can also significantly impact the importance of zonal flow in affecting transport level. Figure 2 shows the suppression effect from zonal flow at magnetic shear $\hat{s}=1.2$ with $R/L_{Te}=6$, T_e/T_i

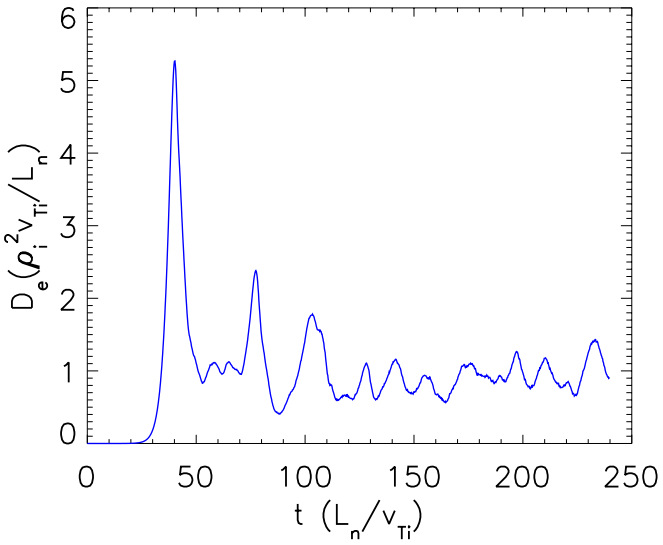

FIG. 3. (Color online) The time evolution of the particle diffusivity at the presence of only one toroidal mode and its complex conjugate in the electrostatic potential.

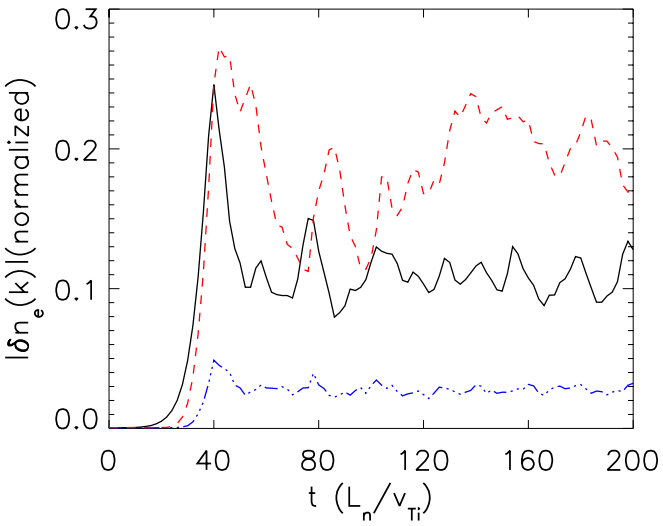

FIG. 4. (Color online) The normalized electron density fluctuation spectrum with Fourier transform in the $x-y$ plane at $z=l_z/2$. The solid line is the primary mode with wave number $k_y=6(2\pi/l_y)$, the dashed line is for the $k_y=0$ mode, the dash-dot line is the mode with wave number $k_y=12(2\pi/l_y)$.

=3, and other parameters the same as those listed above. For low magnetic shear like $\hat{s}=0.8$ or lower, the zonal flow has negligible effect on the transport as shown by Fig. 17 in Ref. 6. At larger magnetic shear, the turbulence is more elongated in radial direction,[6] so that the streamer is easier to be broken by zonal flows. Hence, the turbulent transport can be suppressed more by zonal flows.

Next, we investigate what causes the instabilities to saturate in the parameter regime where zonal flows are unimportant. That is, $T_e/T_i=3.0$, $R/L_{Te}=6$, $\hat{s}=0.8$, and other parameters are the same as above. The linear spectrum with this parameter set was shown in Fig. 1 of Ref. 6. We have carried out simple numerical tests, in which only one toroidal mode $\delta\phi(k_y)$ and its complex conjugate $\delta\phi^*(k_y)$ are retained in the electrostatic potential, and we call these modes the "primary mode" (labeling it as $\delta\phi_p$ with a subscript "p"), where k_y is the wave number in the y direction. In the simulation, we choose one of the linearly dominant modes, the sixth harmonic $k_y\rho_i=0.59$, as the primary mode. But the generation of zonal density is always observed if one of the other linearly unstable modes is kept, say, $k_y\rho_i$ varying from 0.2 to 0.8.

Note that although only a single $|k_y|$ mode is retained in the field quantities, no filtering is done for the distribution function, represented in PIC simulations by the random position of particles and their weights. Thus, Fourier components of the distribution function other than those retained in the field can be nonlinearly generated. A reasonable nonlinear saturation level of the single mode is observed as shown in Fig. 3. It is found that the electron density spectrum reveals that the linearly stable mode with wave number $k_y=0$ is generated at a level comparable to the primary mode δn_p, where δn_p is the normalized electron density fluctuation of the primary mode. This is shown in Fig. 4. This density spectrum is obtained by applying Fourier transform in the $x-y$ plane at $z=l_z/2$. The solid line is the primary mode, the dashed line is for the $k_y=0$ mode, and the dash-dot line is the mode with wave number twice of that of primary mode. The Fourier component of the normalized electron density fluctuation δn_e (in the following, we will drop the "e" for convenience) with wave number $k_y=0$ in general varies with z, the coordinate along **B**, and contains different k_z (wave number in the z direction) components, but the $k_z=0$ component dominates. This is shown in Fig. 5. We refer to the $k_y=0$, $k_z=0$ [or $(n,m)=(0,0)$, (n,m) being the toroidal and poloidal mode number] component of the normalized density fluctuation as the *zonal density* (labeling it as δn_z). Since this component dominates the density spectrum and no other toroidal modes are present, we hypothesize that its generation and

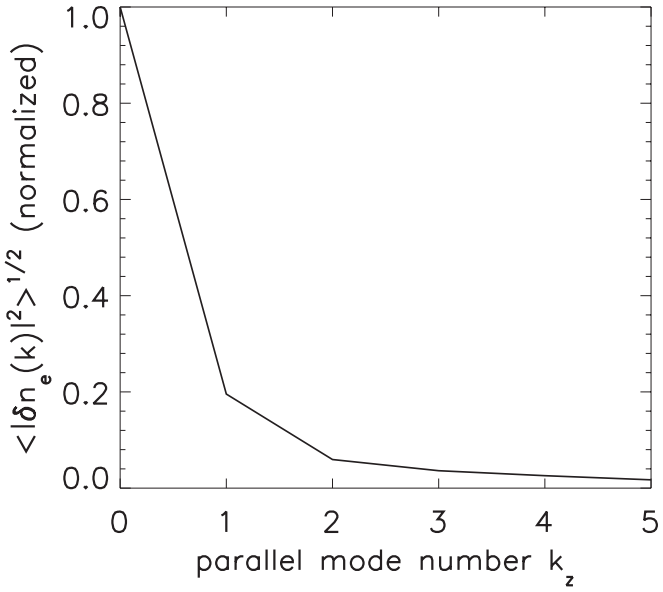

FIG. 5. The spectrum of the normalized electron density fluctuation component $\delta n(k_y=0)$ in parallel direction.

growth to large amplitude are the main nonlinear saturation mechanism. In the following section, we will explain its generation and impact on the primary mode using a mode-coupling model.

III. ZONAL DENSITY GENERATION VIA MODE COUPLING

As discussed in Sec. II, there are parameter regimes, e.g., cold ions relative to electrons where zonal flow is unimportant and a saturated turbulent stationary state is achieved in the absence of zonal flow. We find the normalized density perturbation $\delta n(k_y=0)$ to be important for nonlinear saturation in such a case. The zonal density is the dominant component of $\delta n(k_y=0)$ and is nonlinearly generated by coupling between the primary mode $\delta\phi_p$ and its complex conjugate. Here we examine the generation mechanism of zonal density and its effect on the primary mode. In toroidal coordinates (r,θ,ζ), the eigenmodes are expressed as[20]

$$\delta\phi(r,\theta,\zeta)=\sum_{m,n} f_{m,n}(r)e^{i(n\zeta-m\theta)}e^{-i\omega t}, \tag{1}$$

where n is the toroidal mode number, m is the poloidal mode number, and $f_{m,n}(r)$ is the mode variation along the radial direction. The zonal density has both poloidal mode number $m=0$ and toroidal mode number $n=0$, depending on r only.

Starting with the nonlinear bounce-averaged drift kinetic equation[21–23] for trapped electrons

$$\left(\frac{\partial}{\partial t}+i\omega_{De}\right)h_e-\frac{c}{B}\nabla\langle\delta\phi\rangle\times\mathbf{b}\cdot\nabla h_e = i(2\epsilon)^{1/2}[\omega-\omega_{*Te}(E)]\frac{e\langle\delta\phi\rangle}{T_e}F_{Me}, \tag{2}$$

where the perturbed electron distribution is defined as $\delta f_e=(e\delta\phi/T_e)F_{Me}+h_e$. F_{Me} is the Maxwellian distribution function, and h_e is the nonadiabatic part of the perturbed electron distribution, $\omega_{*Te}(E)=\omega_{*e}[1+\eta_e(E/T_e-3/2)]$, $\omega_{*e}=k_\theta\rho_s C_s/L_n$, $\eta_e=d\ln T_e/d\ln n_0$, where $C_s=\sqrt{T_e/m_i}$, $\rho_s=C_s/\Omega_i$, n_0 is the total electron density, and ω_{De} is the trapped-electron precessional drift frequency which depends on energy.[21,22]Next, we take the density moment of Eq. (2)[23]

$$\left(\frac{\partial}{\partial t}-C_s\rho_s\nabla\langle\phi\rangle\times\mathbf{b}\cdot\nabla\right)\delta n = i(2\epsilon)^{1/2}(\omega-\omega_{*e})\langle\phi\rangle-i\omega_{de}\delta p_e, \tag{3}$$

where $\phi=e\delta\phi/T_e$, $\delta n=\int d^3v h_e/n_0$, and $\delta p_e=\int d^3v Eh_e/n_0T_e \sim \delta n+\delta T_e/T_e$. We assume $\delta p_e=\delta n$ and neglect the $\delta T_e/T_e$ term, which is important for determining the proper linear frequency and growth rate. However, here we are interested in the nonlinear generation of the zonal density and will assume the linear theory is known.

We keep a single unstable toroidal mode (the primary mode with mode number n_p) and its complex conjugate, and this is the linearly unstable mode that grows, couples to itself, and generates the zonal density

$$\delta\phi_p(r,\theta,\zeta,t)=\sum_m f_{m,n_p}(r)e^{i(n_p\zeta-m\theta)}e^{-i\omega t+\gamma t}, \tag{4}$$

Linearizing Eq. (3), the relation between the density and electrostatic potential field of the primary toroidal mode is given by

$$\left(\frac{\partial}{\partial t}+i\omega_{de}\right)\delta n_p=i(2\epsilon)^{1/2}(\omega-\omega_{*e})\phi_p, \tag{5}$$

where $\phi_p=e\delta\phi_p/T_e$ is the normalized electrostatic potential.

From this model, the linear relationship between density and the electrostatic potential of the primary mode is

$$\frac{|\delta n_p|}{|\phi_p|}=(2\epsilon)^{1/2}\frac{|(\omega-\omega_{*e})|}{\sqrt{(\omega_{de}-\omega)^2+\gamma^2}}. \tag{6}$$

The zonal density is linearly stable, so its time evolution only depends on the $E\times B$ nonlinear term $C_s\rho_s\nabla\langle\phi\rangle\times\mathbf{b}\cdot\nabla\delta n$. The generation of zonal density can be written as

$$\frac{\partial}{\partial t}\delta n_z(r)-C_s\rho_s\nabla\langle\phi\rangle\times\mathbf{b}\cdot\nabla\delta n=0. \tag{7}$$

The Fourier transform of the nonlinear term $C_s\rho_s\nabla\langle\phi\rangle\times\mathbf{b}\cdot\nabla\delta n$ is $\Sigma_{\mathbf{k}=\mathbf{k}_1+\mathbf{k}_2}C_s\rho_s i\mathbf{k}_1\times\mathbf{b}\cdot i\mathbf{k}_2\langle\phi(\mathbf{k}_1)\rangle\delta n(\mathbf{k}_2)$, which indicates a mode-coupling process. In the toroidal coordinates, Eq. (7) is equivalent to the following expression with the presence of only the primary mode and its complex conjugate:

$$\frac{\partial}{\partial t}\delta n_z(r)-\frac{C_s\rho_s}{r}\left(\frac{\partial\phi_p}{\partial\theta}\frac{\partial\delta n_p}{\partial r}-\frac{\partial\phi_p}{\partial r}\frac{\partial\delta n_p}{\partial\theta}\right)=0. \tag{8}$$

Since the zonal density has toroidal mode number equal to 0, only the coupling between ϕ_p and δn_p* or ϕ_p* and δn_p needs to be considered. Inserting the linear relation between ϕ_p and δn_p shown in Eq. (5), using Eq. (4), and keeping the dominant poloidal mode $m=n_pq_0$ gives

$$\frac{\partial\delta n_z(r)}{\partial t}+\frac{ce}{BT_e}\frac{m}{r}\frac{\partial(ff^*)}{\partial r}\sqrt{2\epsilon}\frac{2\gamma(\omega_{*e}-\omega)}{\gamma^2+(\omega-\omega_{de})^2}e^{2\gamma t}=0. \tag{9}$$

To compare with the simulation, we assume periodic boundary conditions in radial direction as used in our flux-tube model and Fourier decompose in r: $f_{m,n_p}(r)=\delta\phi_p\Sigma_{k_r}\sin(k_rr+\theta_0)$, where $|\delta\phi_p|$ is the electrostatic potential amplitude with toroidal number n_p and θ_0 is an arbitrary phase. Considering the dominant radial wave number k_r, the time dependence of zonal density in the early nonlinear regime is

$$\delta n_{z,kr}=(2\epsilon)^{1/2}\frac{ce}{BT_e}\frac{m}{r}k_r|\delta\phi_p|^2\frac{(\omega_{*e}-\omega)}{\gamma^2+(\omega-\omega_{de})^2}\sin(2k_rr+2\theta_0)e^{2\gamma t}. \tag{10}$$

From Eq. (10), we immediately see that the zonal density is a purely growing mode with the growth rate twice that in the primary unstable mode. The dominant radial wave number k_r is also twice that in the primary unstable mode and the toroidal mode number $n=0$. All are the immediate consequence of the coupling between the primary mode with its complex conjugate. Shortly, we will compare the generation of zonal

density between this model and the simulation results after we describe how this nonlinearly generated zonal density δn_z, in turn, saturates the primary mode.

Next, the nonlinear saturation mechanism for the situation due to zonal density (when zonal flow is unimportant) is discussed. After nonlinearly generated during the coupling process, the zonal density then feeds back and can stabilize the primary mode leading to nonlinear saturation. The nonlinear evolution of the primary mode is obtained from Eq. (3)

$$\left(\frac{\partial}{\partial t}+i\omega_{de}\right)\delta n_p - i\sqrt{2\epsilon}(\omega-\omega_{*e})\phi_p - C_s\rho_s\nabla\langle\phi_p\rangle \times \mathbf{b}\cdot\nabla\delta n_z = 0. \tag{11}$$

Combining with Eq. (5), but still using the toroidal eigenvalues, the explicit form of Eq. (3) is

$$\left(\frac{\partial}{\partial t}+i\omega_{de}\right)\delta n_p - i\sqrt{2\epsilon}(\omega-\omega_{*e})\phi_p - C_s\rho_s\left(\frac{\partial\phi_p}{\partial\theta}\frac{\partial\delta n_z}{\partial r}-\frac{\partial\phi_p}{\partial r}\frac{\partial\delta n_z}{\partial\theta}\right)=0. \tag{12}$$

From Eq. (10), we can see $\partial\delta n_z/\partial\theta=0$. Inserting the expression of $\delta\phi_p$ in Eq. (4), the saturation level can be predicted from Eq. (12) for the mode with dominant radial wave number and poloidal wave number.

When saturation happens, $\gamma_{nl}\sim 0$ and $\partial\delta n_p/\partial t\sim -i\omega\delta n_p$, we assume the frequency ω as the linear frequency. Solving Eq. (12), we can obtain the saturation level of the dominant radial component of zonal density as

$$|\delta n_{z,kr}| = \frac{\gamma_L}{\sqrt{2}k_r L_n\omega_{*e}}\frac{|\delta n_p|}{|\phi_p|}. \tag{13}$$

Since the electrostatic potential amplitude of the primary mode is related to the zonal density amplitude by Eq. (10), the saturation level of the primary mode can be determined

$$|\phi_p| = ((\omega-\omega_{de})^2\gamma_L^2+\gamma_L^4)^{1/4}\frac{1}{\sqrt{2}k_r L_n\omega_{*e}}. \tag{14}$$

Note that Eqs. (13) and (14) are really only valid in the early nonlinear phase, so the prediction for the saturation should only work for the "first peak" in the simulation.

The prediction of the saturation level is actually a result from the balance between the linear driving term and the $E\times B$ nonlinear term. If the mode frequency is close to the precessional drift frequency of the trapped electrons, i.e., $|\omega-\omega_{de}|\ll\gamma_L$, the saturation level of zonal density and the primary mode will be the same order as the result from the fluid theory $\gamma_L/k_r L_n\omega_{*e}$.[24] Besides, the saturation level of zonal density is related to the electron density fluctuation to the electrostatic potential ratio of the primary mode, which can be directly evaluated from the simulation without knowing the analytically linear theory.

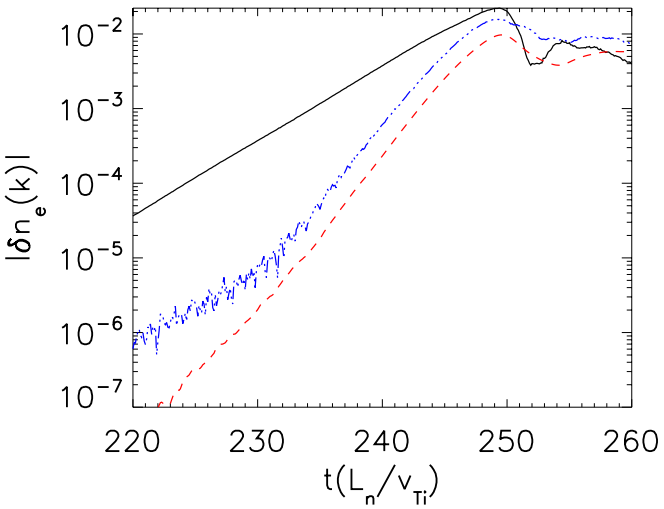

FIG. 6. (Color online) The time evolution of the absolute amplitude of the normalized electron density fluctuation for different modes. The solid line is for the primary mode δn_p, the dash-dot line is for the mode with $k_y=0$ but including all $k_z's$, the dashed line is for the zonal density with dominant radial component $\delta n_{z,k_r}$.

IV. NONLINEAR GENERATED ZONAL DENSITY: COMPARISON WITH THE SIMULATION RESULTS

We now compare the simple mode-coupling theory in Sec. III with simulation results from GEM. GEM uses fully kinetic ions and electrons with split-scheme applied on electrons, which ensures numerical stability at larger time steps.[25] The perturbed electron distribution is defined as $\delta f_e=\varepsilon_g(e\delta\phi/T_e)F_{Me}+h_e'$, where ε_g is a small parameter and h_e' is the perturbed electron distribution of the nonadiabatic part. The simulation parameters are the same as in Sec. II with electron temperature gradient $R/L_{Te}=6$, electron to ion temperature ratio $T_e/T_i=3$, and magnetic shear $\hat{s}=0.8$. In the single toroidal mode test, only the linearly most unstable mode $k_y=6(2\pi/l_y)$ is kept (we call it the primary mode) in the electrostatic potential. To clearly address the doubling in radial mode number k_r, the component with $k_r=0$ in the electrostatic potential is set to zero. The nonlinear terms are not turned on until the linear eigenmode is fully dominant. To compare the simulation with the mode-coupling model, the assumption of the primary perpendicular wave number $k_y=n_p q_0/r=m/r$ is used.

First, we examine the generation of zonal density. Figure 6 shows the time evolution of the normalized amplitude of zonal density (dash line), $\delta n(k_y=0)$ (dash-dot line), and the primary unstable mode δn_p (solid line) on a Log scale. A doubling in the growth rate of zonal density compared with that of the primary mode is observed which agrees with the mode-coupling model. The growth rate of mode $\delta n(k_y=0)$ is the same as zonal density, which is not a surprise because the dominant component of $\delta n(k_y=0)$ is zonal density as shown in Fig. 5. In the radial direction, the dominant radial wave number of the primary unstable mode is $k_r=2\pi/l_x$ and the dominant radial wave number of zonal density is $k_r=2(2\pi/l_x)$ in agreement with the mode-coupling theory. The time evolution of the real part of zonal density does not oscillate early on, that is, zonal density is purely growing,

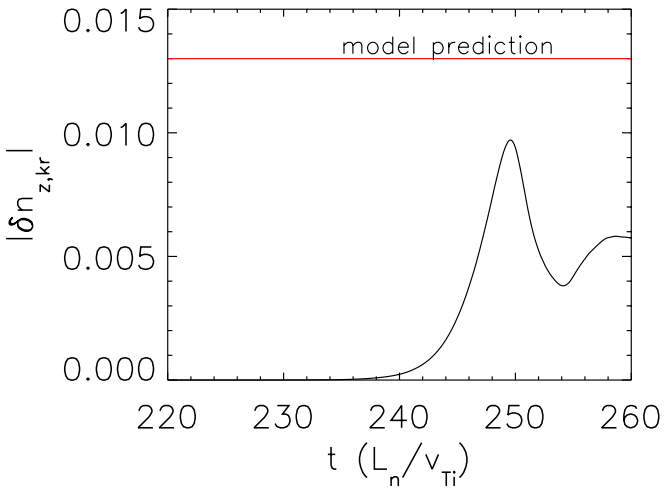

FIG. 7. (Color online) The comparison in saturation amplitude of zonal density with dominant radial wave number between the model prediction and the simulation result.

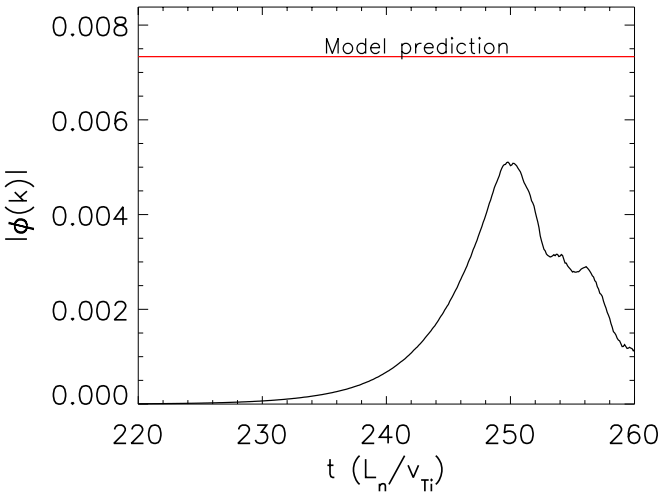

FIG. 8. (Color online) The comparison in normalized electrostatic potential saturation amplitude of the primary mode with dominant radial wave number between the mode prediction and the simulation result.

again in agreement with the theory. These features observed in the simulation show a good agreement with the model Eq. (10).

Next, we will compare the saturation level obtained from the simulation with the predicted value from the mode-coupling model. We note that the normalized electron density $\delta n'$ in the GEM simulation is not the same as δn in the model due to the expansion about the adiabatic response. To compare with the simulation, we need to convert the relation between the electron density and electrostatic potential in the mode-coupling model to our simulation model. As mentioned above, we include fully kinetic electrons using a split-weight scheme,[9] i.e., the perturbed electron distribution is $\delta f_e=\varepsilon_g(e\delta\phi/T_e)F_{Me}+h'_e$. The perturbed electron distribution function for these two models should be the same. The relation between density and electrostatic potential in our simulation can be obtained according to the mode-coupling model

$$\frac{|\delta n'_p|}{|\phi_p|}=\frac{|\delta n_p|}{|\phi_p|}+(1-\varepsilon_g). \tag{15}$$

The notation "′" means simulation result and $\phi_p=e\delta\phi_p/T_e$. Comparing the density and electrostatic potential relation based on the linearly most unstable mode $k_y=6(2\pi/l_y)$, we get the value of $|\delta n'_p|/|\phi_p|=1.95$ by directly measuring the simulation result in the linear phase, which is from the fully kinetic model as used in GEM. But from Eq. (6) combined with Eq. (15), namely, simulation parameters and the mode frequency obtained from linear simulation will give a number with a factor of 2 difference from the direct measurement. This is not a big surprise, since the CTEM requires a kinetic linear theory. We take an assumption in $\delta p_e=\delta n$ by neglecting the term $\delta T_e/T_e$, which is actually on the same order with the term δn. Since this neglected term only has contribution to the linear theory, we can predict the saturation level in the initial nonlinear regime from Eq. (13) by taking the linear relation between δn_p and ϕ_p from the simulation instead of the linear model. The saturation of the zonal density with dominant radial wave number $k_r=2(2\pi/l_x)$ is shown in Fig. 7. According to our linear simulation result, the relation between density and electrostatic potential of the primary mode in the model is given by $|\delta n_p|/|\phi_p|=1.05$. Next, by using Eq. (13), the mode-coupling model will give the saturation level of zonal density as 0.013, which is within 30% accuracy compared with the simulation shown in Fig. 7.

The saturation level of the primary unstable mode is predicted by Eq. (14). Since the electrostatic potential in the simulation is the same as that in the model, we can compare these results directly. Figure 8 shows the saturation process of the primary electrostatic potential. Compared with the prediction value obtained from Eq. (14), the simulation result shows a good agreement with the model. Though agreement between nonlinear theory and simulation is good, a few caveats should be mentioned: (i) The saturation level predicted from this mode-coupling model is only valid for the early nonlinear regime, which corresponds to the "first peak" in our simulation (like Fig. 8). (ii) Besides the zonal density, the linearly stable mode δn with the wave number twice that in the primary mode is also nonlinearly generated (shown in Fig. 4), and it could also affect the nonlinear saturation of the primary mode.

V. NONLINEAR ENERGY CASCADE

In this section, we will discuss the nonlinear inverse cascade in the wavelength spectrum found in gyrokinetic simulations of CTEM turbulence. The time evolution of the averaged wave number $\bar{k}_y$ is measured, following what is done in Ref. 15 for ITG turbulence. The averaged wave number $\bar{k}_y$ is defined as $\bar{k}_y=[\Sigma_{k_x,k_y}k_y\delta\phi(k_x,k_y)^2]/[\Sigma_{k_x,k_y}\delta\phi(k_x,k_y)^2]$. The time evolution of the averaged wave number and the electrostatic potential is shown in Fig. 9. It is observed that $\bar{k}_y$ goes down by a factor 2 (the solid line) at a time regime where the saturation of CTEM turbulence (dashed line) occurs. In the linear phase, the $\bar{k}_y$ is dominated by the linearly most unstable modes with larger wave number. In the nonlinear

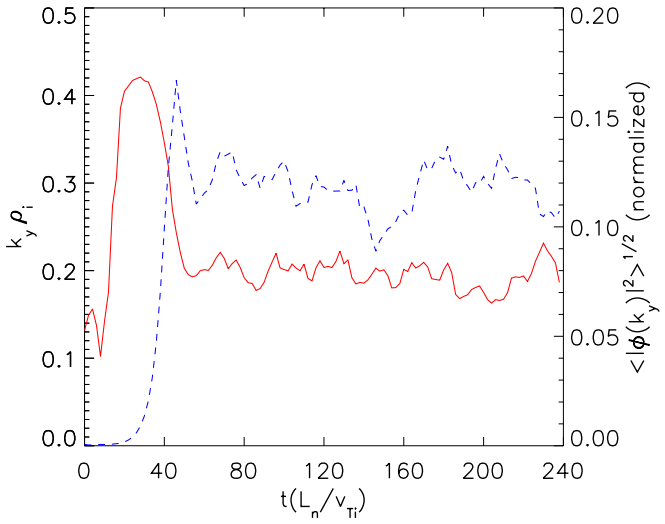

FIG. 9. (Color online) The time evolution of the averaged wave number $\bar{k}_y$ (solid line) and the electrostatic potential of the primary mode (dashed line).

phase, the $\bar{k}_y$ is later dominated by modes with lower wave number. This is similar to what was observed in the ITG turbulence.[15] In this plot, the zonal flows are not shown and the parameters are the same as those used in Sec. IV.

The downward shift in the nonlinear spectrum has been studied both numerically[14,15] and theoretically.[22] As discussed in Sec. III, we have already shown that when only one toroidal mode is kept in the electrostatic potential, the simulation will saturate due to zonal density generation and feedback on the primary unstable mode. But the saturation depends on the growth rate of the primary toroidal mode. According to this theory, the toroidal modes with longer wavelength should saturate much later, due to the smaller growth rate. This result is shown by simulation in Fig. 10(a). In this plot, the dashed line indicates the time evolution of the electrostatic potential with wave number $k_y\rho_i=0.6$ and the solid line indicates the time evolution of the electrostatic potential with wave number $k_y\rho_i=0.1$. The mode $k_y\rho_i=0.1$ is weakly unstable, and we can see that when saturation has occurred for the mode $k_y\rho_i=0.6$, the mode $k_y\rho_i=0.1$ is still stable. However, when all toroidal modes are kept in the electrostatic potential, the energy will cascade from the mode with larger wave number to the mode with lower wave number, which is shown in Fig. 10(b). The amplitude of mode $k_y\rho_i=0.1$ is strongly enhanced while the amplitude of the mode $k_y\rho_i=0.6$ is suppressed. The saturation level of the mode $k_y\rho_i=0.1$ is much higher than mode $k_y\rho_i=0.6$. We explain the exchange of energy in these two modes as a nonlinear mode-coupling process by the interaction between the density fluctuation and electrostatic potential, which is similar to the zonal density impacting the primary mode. Taking a simple example, the linearly unstable toroidal modes with wave number $k_y\rho_i=0.6$ and $k_y\rho_i=0.5$ behave as the primary modes. The coupling between the mode $k_y\rho_i=0.6$ and the complex conjugate of mode $k_y\rho_i=0.5$ will drive the linearly stable mode $k_y\rho_i=0.1$ to grow. This mode-coupling process can only occur during the nonlinear evolution.

Finally, an interesting observation is found by keeping only two toroidal modes $k_y\rho_i=0.1$ and $k_y\rho_i=0.6$ and their complex conjugates in the electrostatic potential. (Note: we have no control of the Fourier modes of the distribution in δf particle simulation.) There is still energy transfer from the linearly unstable mode $k_y\rho_i=0.6$ to the stable mode $k_y\rho_i=0.1$ as shown in Fig. 10(c). The linearly stable mode $k_y\rho_i=0.1$ saturates at the same time but with a higher level compared with the linearly unstable mode $k_y\rho_i=0.6$. Although this result looks similar to that shown in Fig. 10(b), there is a crucial distinction in the nonlinear physics. Figure 10(c) should be a result from wave-particle interaction instead of mode-coupling. Because the linearly stable mode $k_y\rho_i=0.1$ cannot be nonlinearly driven unstable by mode-coupling process without a third mode, the observed nonlinear cascading process is actually caused by different physical mechanisms. Further work will address this effect.

VI. SUMMARY

In this paper, we study three nonlinear saturation mechanisms for CTEM turbulence. Zonal flows often are important in saturating CTEM turbulence and suppressing transport, but the effect is sensitive to the local plasma parameters. Specifically, the importance of zonal flow is especially sensitive to electron temperature gradient, electron to ion tem-

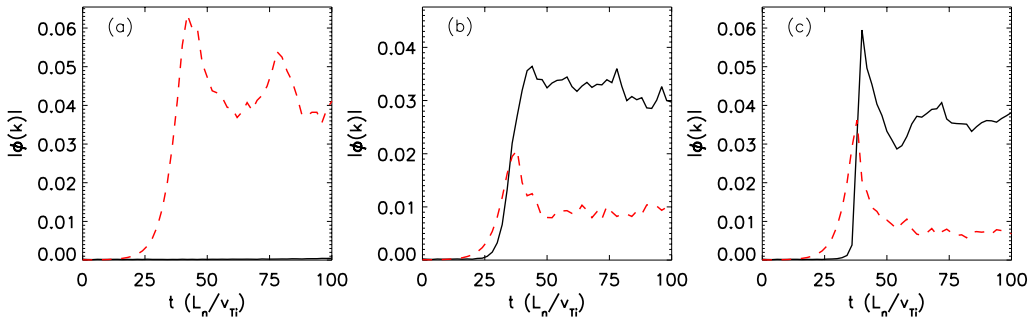

FIG. 10. (Color online) (a) The time evolution of the normalized electrostatic potential of two modes $k_y=6(2\pi/l_y)$ (dashed line) and $k_y=2\pi/l_y$ (solid line, which is hard to see since it is very close to the x axis) from two separated simulations. Only one mode is kept in electrostatic potential for each simulation. (b) The time evolution of the normalized electrostatic potential of two modes $k_y=6(2\pi/l_y)$ (dashed line) and $k_y=2\pi/l_y$ (solid line) from one simulation. All modes are retained in the electrostatic potential. (c) The time evolution of the normalized electrostatic potential of two modes $k_y=6(2\pi/l_y)$ (dashed line) and $k_y=2\pi/l_y$ (solid line) from one simulation. Only these two modes are retained in the electrostatic potential.

perature ratio, and magnetic shear. The importance of zonal flows is well explained by the $E \times B$ shearing rate criterion. For the parameter regime where zonal flows are found to be unimportant, zonal density generation and its feedback on linearly unstable modes are found to dominate nonlinear saturation. A simple mode-coupling model is shown to explain zonal density generation and nonlinear saturation. We considered a mode-coupling analysis where one toroidal linearly unstable mode generates the zonal density and good agreement between the model and numerical simulation results was obtained. Furthermore, another important saturation mechanism, namely inverse energy cascade, is also reported. The correlation between the downshift in the wavelength spectrum and the CTEM turbulent saturation is observed, which can be partially explained by the mode-coupling model as well.

ACKNOWLEDGMENTS

We thank G. W. Rewoldt and W. W. Lee for helpful discussions.

This work is supported by the Department of Energy Scientific Discovery through Advanced Computing Center for Plasma Edge Simulation.

[1] T. A. Davydova, J. Weiland, and A. I. Yakimenko, Phys. Plasmas **9**, 4623 (2002).
[2] P. W. Terry and R. Gatto, Phys. Plasmas **13**, 062309 (2006).
[3] D. R. Ernst, P. T. Bonoli, P. J. Catto, W. Dorland, C. L. Fiore, R. S. Granetz, M. Greenwald, A. E. Hubbard, M. Porkolab, M. H. Redi, J. E. Rice, and K. Zhurovich, Phys. Plasmas **11**, 2637 (2004).
[4] T. Dannert and F. Jenko, Phys. Plasmas **12**, 072309 (2005).
[5] J. E. Kinsey, R. E. Waltz, and J. Candy, Phys. Plasmas **13**, 022305 (2006).
[6] J. Lang, Y. Chen, and S. E. Parker, Phys. Plasmas **14**, 082315 (2007).
[7] J. C. DeBoo, S. Cirant, T. C. Luce, A. Manini, C. C. Petty, F. Ryter, M. E. Austin, D. R. Baker, K. W. Gentle, C. M. Greenfield, J. E. Kinsey, and G. M. Staebler, Nucl. Fusion **45**, 494 (2005).
[8] F. Ryter, C. Angioni, A. G. Peeters, F. Leuterer, H.-U. Fahrbach, and W. Suttrop, Phys. Rev. Lett. **95**, 085001 (2005).
[9] Y. Chen and S. E. Parker, J. Comput. Phys. **189**, 463 (2003).
[10] Y. Chen and S. E. Parker, J. Comput. Phys. **220**, 839 (2007).
[11] M. A. Beer, S. C. Cowley, and G. W. Hammett, Phys. Plasmas **2**, 2687 (1995).
[12] T. Hahm, Phys. Plasmas **1**, 2940 (1994).
[13] T. S. Hahm and K. H. Burrell, Phys. Plasmas **2**, 1648 (1995).
[14] S. E. Parker, W. W. Lee, and R. A. Santoro, Phys. Rev. Lett. **71**, 2042 (1993).
[15] W. X. Wang, T. S. Hahm, W. W. Lee, G. Rewoldt, J. Manickam, and W. M. Tang, Phys. Plasmas **14**, 072306 (2007).
[16] A. M. Dimits, T. J. Williams, J. A. Byers, and B. I. Cohen, Phys. Rev. Lett. **77**, 1 (1996).
[17] Z. Lin, T. S. Hahm, W. W. Lee, W. M. Tang, and R. B. White, Science **281**, 1835 (1998).
[18] P. N. Guzdar, R. G. Kleva, and L. Chen, Phys. Plasmas **8**, 459 (2001).
[19] P. H. Diamond, S.-I. Itoh, K. Itoh, and T. S. Hahm, Plasma Phys. Controlled Fusion **47**, R35 (2005).
[20] L. Chen and C. Z. Cheng, Phys. Fluids **23**, 2242 (1980).
[21] F. Y. Gang and P. H. Diamond, Phys. Fluids B **2**, 2976 (1990).
[22] T. S. Hahm and W. M. Tang, Phys. Fluids B **3**, 989 (1991).
[23] T. S. Hahm and W. M. Tang, Phys. Plasmas **3**, 242 (1996).
[24] J. Weiland, Phys. Scr., T **82**, 84 (1999).
[25] Y. Chen and S. E. Parker, Phys. Plasmas **8**, 2095 (2001).